A NONLINEAR MODEL FOR VELOCITY ESTIMATION FROM INFRARED IMAGE SEQUENCES

Wei Chen

Naval Research Laboratory, Remote Sensing Division, Code 7233, 4555 Overlook Ave. S.W., Washington, D.C. 20375, USA

Commission VIII, WG VIII/9

KEY WORDS: Ocean Current, Surface Velocity, Velocity Estimation, Motion Estimation, infrared images, AVHRR Images

ABSTRACT:

Velocity estimation using tracer conservation or heat flow equation based on infrared image sequence is one of the most challenging inverse problems in geosciences and remote sensing applications. In this paper, a new nonlinear model has been created for estimating top surface velocity from an infrared image sequence. The differential form of tracer conservation or heat flow equation is replaced by a temporal integral form of the heat flow conservative constraint equation in which the initial and final states of flow terms are associated with only two time-varying frames at time t_1 and t_2. Iterative equations with Gauss-Newton and Levenberg-Marguardt algorithms for the estimation of the top surface velocity are formulated based on the temporal integral form of the heat flow equation, modelling the velocity field, and a nonlinear least-squares model. The solution of a numerical model is used as a benchmark to exam the new estimator. Both angular and magnitude error measurements based on the synthetic surface heat flow from the numerical model demonstrate that the performance of the new approach with the nonlinear model are much better than the results of using a linear model of the tracer conservation or heat flow equation. One sequence of NOAA AVHRR images taken in the New York Bight fields is also used to demonstrate the performance of the nonlinear inverse model.

1. INTRODUCTION

Estimation of surface velocity from an infrared image sequence is one of the most challenging inverse problems in studies of ocean circulations. Scientists have used a number of techniques to solve the inverse problems, but two procedures have achieved prominence over the last few decades. The first is the Maximum Cross Correlation (MCC) algorithm (cf. Leese and Novak, 1971; Emery *et al.* 1986), which is a feature-tracking technique that is used extensively by oceanographers to process satellite data for surface velocities. Another technique is the inversion of the heat or optical flow equation for the velocity vector (cf. Horn and Shunck 1981; Kelly 1989; Kelly and Strub 1992; Ostrovskii and Piterbarg 1995, 2000; Vigan *et al*. 2000; Zavialov *et al*. 1998; Cote and Tatnall 2007).

Marcello *et al.* (2008) performed evaluation and detailed studies of popular motion estimation techniques in computer vision field applying to tracking oceanographic thermal structures. Their works indicate that Luscas-Kanade (1981), (1984) is the only differential approach tested that provided a reasonable error performance in tracking geography flow motion, whereas Black-Anandan (1996) achieved only angular accuracy.

An alternate strategy is proposed by Chen *et al.*, (2008) to solve the inverse problem by representing heat flow with bilinear polynomials over the distance of several pixels (a sub-image). They estimated top surface velocities with the heat flow conservation equation. The velocity is chosen as an optimal fit to the heat flow equation, and is thus globally valid over the image domain. Simultaneous solutions for this field and the velocity yield a Global Optimal Solution (1st-order GOS). A higher order GOS in which the velocity field is expanded by surface B-Splines Function to solve the optical or heat flow equation is also developed by Chen (2010).

In remote sensing applications that attempt to estimate the surface velocity from thermal satellite-born image sequences, the time difference between two images is usually in the order of several hours (Chen *et al.*, 2008, 2010), and the displacement of motion is usually somewhere between zero and several pixels. The heat flow equation in the GOS algorithms is a differential form of the conservative heat flow constraint (first-order Taylor expansion) and holds only for an infinitesimal motion. Using the differential form of the heat equation for large scale displacement field estimation may create errors in real-world applications. To improve the performance of the velocity estimation from an infrared image sequence, we utilize a temporal integral form of the conservative heat flow equation to replace the differential form and create a nonlinear system in this paper for the top surface velocity estimation.

This paper is organized as follows: In section 2, a set of system equations with the inverse model are derived. Section 3 introduces algorithms that are applied to the design for this velocity estimator. Section 4 deals with the validation of the nonlinear inverse model by deriving velocity from synthetic tracer motion within a numerical ocean model. Next, we investigate the robustness of the velocity retrievals with detailed statistical comparisons between the current fields obtained by the proposed estimator and numerical ocean model. We apply the nonlinear inverse model to one AVHRR image pair from the North Atlantic Ocean. Finally, conclusions are drawn in the last section.

2. A NONLINEAR MODEL

2.1 Heat Flow Equation

The heat flow of an image sequence is a set of vector fields, relating each image to the next. Each vector field represents the apparent displacement of each pixel from image to image. If the

evolution of the heat field in a two-dimensional surface of ocean is conserved, the conserved heat flow must be governed by the following equation (Horn-Shunck 1981; Kelly 1989)

$$\frac{dT}{dt} = (\frac{\partial}{\partial t} + \mathbf{v} \cdot \nabla)T = S \, , \, (1)$$

where $T = T(x, y, t)$ is the temperature of the heat flow with regard to the x, and y coordinates, and time t. The heat flow vector is defined by $\mathbf{v}(x, y, t) = (u, v)$. The variable $S = S(x, y)$ is a group term of source, noise, and diffusion containing the effects of air-sea interaction and turbulent processes within the mixed-layer (see, e.g., Kelly 1989, and Chen *et al.*, 2008). Equation (1) is called the heat flow or tracer conservation equation.

Integrating equation (1) from time t_1 to t_2, we have a Temporal Integral form of the Heat Flow Constraint equation (TIHFC)

$$TIHFC = T(x + \Delta x, y + \Delta y, t_2) - T(x, y, t_1) + s(x, y) = 0 \, , \, (2)$$

where x and y are fixed position coordinates at time $t = t_1$, Δx and Δy are two components of the displacement field, and the temporal integral of group of the source, noise, and diffusion terms is denoted by

$$s(x, y) = -\int_{t_1}^{t_2} S(x, y)dt \cdot$$

For a special case, if the group term of the source, noise, and diffusion are negligible, equation (2) becomes the displacement frame difference equation (Robbins and Netravali, 1983) as follows

$$DFD = T(x + u\Delta t, y + v\Delta t, t_2) - T(x, y, t_1) \cdot (3)$$

There are three in (2) or two in (3) unknown variables in an image sequence, so the problem is under-determined, and extra constraints must be imposed in order to arrive at a solution.

2.2 Expansion of Velocity Field

In order to solve the inverse problem for the optical or heat flow fields using equation (1) based on time varying frames, we utilize an efficient approach in which we expand the velocity field as bilinear polynomial functions or two-dimensional B-Splines functions (Chen *et al.*, 2008, 2010). To reduce the computational complexity, we utilize the bilinear polynomial functions to present the velocity field in this topic.

Any two-dimensional function can be expressed by bilinear polynomial

$$f(x, y) = \sum_{\alpha=0}^{1} \sum_{\beta=0}^{1} f_{p+\alpha n_x, q+\beta n_y} H_{p+\alpha n_x, q+\beta n_y}(x, y) \, , \, (4)$$

where $f_{ij} = f(i, j)$, preset parameters n_x and n_y are the number of interpolation points on x and y directions as shown in Figure 1, and quantized indices p and q on nodes are functions of x and y and are given by

$$\{p, q\} = \{n_x \lfloor \frac{x}{n_x} \rfloor, n_y \lfloor \frac{y}{n_y} \rfloor\} \, ,$$

where $\lfloor \ \rfloor$ denotes an integer operator. The function $H_{a,b}(x, y)$ is defined by

$$H_{a,b}(x, y) = \frac{1}{n_x n_y} \begin{cases} (n_x - x + p)(n_y - y + q) & (a = p \cap b = q) \\ (x - p)(n_y - y + q) & (a = p + n_x \cap b = q) \\ (n_x - x + p)(y - q) & (a = p \cap b = q + n_y) \\ (x - p)(y - q) & (a = p + n_x \cap b = q + n_y) \end{cases}.$$

The two components velocity field and the source term on image scene can be expressed by the following discretional forms of the bilinear polynomial functions with first order continuity that holds for all $N_x \times N_y$ image globally

$$\{u_{ij}, v_{ij}, s_{ij}\}$$
$$= \sum_{\alpha=0}^{1} \sum_{\beta=0}^{1} \{u_{p+\alpha n_x, q+\beta n_y}, v_{p+\alpha n_x, q+\beta n_y}, s_{p+\alpha n_x, q+\beta n_y}\} H_{p+\alpha n_x, q+\beta n_y}(i, j) \, . \, (5)$$

All velocity and source term off nodes (blue color points shown in Fig. 1) can be calculated by equation (5) using the velocity and source term on node points that are expressed as u_{pq}, v_{pq} and s_{pq}. The TIHFC equation in (2) becomes

$$TIHFC_{ij} = T(i + u_{ij}\Delta t, j + v_{ij}\Delta t, t_2) - T_{ij}(t_1) + s_{ij} \, , \, (6)$$

where $TIHFC_{ij}$ is an error of the temporal integral form of the heat flow constraint equation. Now, the equation (3) is no longer local, and all unknown velocities on nodes are connected with each other in whole image scene shown in Figure 1.
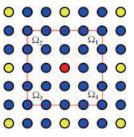

Figure 1. Bilinear square pixel sub-arrays ($n_x = 3$ and $n_y = 3$) with 9 node points in which yellow (p, q) and red (k, l) node pixels are unknown velocities that are mapped onto an image scene.

The preset parameter $n = n_x = n_y$ is the degree of over-constraint of the system. When $n \geq 2$, the system is over-constrained for all unknown velocity field u_{pq}, v_{pq}, and the group term s_{pq}. We will solve this over-constrained system with a global optimal approach in next section.

2.3 A Nonlinear Least-Squares Model

Considering the existence of quantization errors and noise during the intensity measurements, the TIHFC equation in (6) is never equal to zero. According to least-squares principle, a chi-squares that is a sum of the total errors in (6) is given by

$$\chi^2 = \sum_{i,j} TIHFC_{ij}^2 \, ,$$

where i and j go over all pixels in $N_x \times N_y$ image ($i \in [0, N_x - 1] \cap j \in [0, N_y - 1]$). Minimizing the chi-squares

function for the given indices k and l for all node points in an image, we have

$$\left\{\frac{\partial \chi^2}{\partial u_{kl}}, \frac{\partial \chi^2}{\partial v_{kl}}, \frac{\partial \chi^2}{\partial s_{kl}}\right\} = 0 .$$

Since

$$\begin{cases} \dfrac{\partial TIHFC_{ij}}{\partial u_{kl}} = \dfrac{\partial T(x, j + v_{ij}\Delta t, t_2)}{\partial x}\bigg|_{x=i+u_{ij}\Delta t} \sum_{\alpha=0}^{1}\sum_{\beta=0}^{1} H_{k,l}(i,j)\delta_{k,p+\alpha n_x}\delta_{l,q+\beta n_y} \\[2mm] \dfrac{\partial TIHFC_{ij}}{\partial v_{kl}} = \dfrac{\partial T(i + u_{ij}\Delta t, y, t_2)}{\partial y}\bigg|_{y=j+v_{ij}\Delta t} \sum_{\alpha=0}^{1}\sum_{\beta=0}^{1} H_{k,l}(i,j)\delta_{k,p+\alpha n_x}\delta_{l,q+\beta n_y} \\[2mm] \dfrac{\partial TIHFC_{ij}}{\partial s_{kl}} = -\sum_{\alpha=0}^{1}\sum_{\beta=0}^{1} H_{k,l}(i,j)\delta_{k,p+\alpha n_x}\delta_{l,q+\beta n_y} \end{cases}$$

, (7)

where the symbol δ_{ij} is the Kronecker-Delta symbol, we can prove

$$\begin{aligned} &\sum_{i,j} TIHFC_{ij}\left\{\frac{\partial TIHFC_{ij}}{\partial u_{kl}}, \frac{\partial TIHFC_{ij}}{\partial v_{kl}}, \frac{\partial TIHFC_{ij}}{\partial s_{kl}}\right\} , \\ &= \sum_{i,j\in\Omega} TIHFC_{ij}\left\{\frac{\partial TIHFC_{ij}}{\partial u_{kl}}, \frac{\partial TIHFC_{ij}}{\partial v_{kl}}, \frac{\partial TIHFC_{ij}}{\partial s_{kl}}\right\} \end{aligned}$$

where the summation denoted in above equations are given by

$$\sum_{i,j\in\Omega} = \sum_{i=k-n_x+1}^{k+n_x-1}\sum_{j=l-n_y+1}^{l+n_y-1} .$$

The regions that the summations go over pixel points (within the red color frame) and some unknown velocities and sources that are mapped onto this image with indices (p, q) and (k, l) are shown in Fig. 1.

Using the optimization conditions and equations (7), a set of over-determined system of equations for the estimation of the surface velocity is given by

$$\begin{cases} \sum_{i,j\in\Omega} TIHFC_{ij}\dfrac{\partial TIHFC_{ij}}{\partial u_{kl}} = 0 \\[2mm] \sum_{i,j\in\Omega} TIHFC_{ij}\dfrac{\partial TIHFC_{ij}}{\partial v_{kl}} = 0 \\[2mm] \sum_{i,j\in\Omega} TIHFC_{ij}\dfrac{\partial TIHFC_{ij}}{\partial s_{kl}} = 0 \end{cases}$$

, (8)

when the parameters $n \geq 2$. The three independent equations in (8) on node points can be degraded back to a single optical or heat flow equation (1) when n is equal to unity.

All velocities u_{pq}, v_{pq}, and s_{pq} on node points can be obtained by solving the nonlinear system equations in (8), and the velocities u_{ij}, v_{ij}, and s_{ij} off node points can be calculated by the interpolation functions in (5). The summations in (8) cover only the unknown velocities u_{kl}, v_{kl}, and s_{kl} and their surrounding nearest neighbor node points as shown in figure 1. The equations in (8) is a nonlinear system of equations, they can be solved by Gauss-Newton and Levenberg-Marguardt algorithms.

2.4 Solving a Nonlinear System of Equations

The velocities u_{kl} and v_{kl} and their surrounded nearest neighbor velocities are implicitly contained in the summations in equation (8) and (6). Using Gauss-Newton algorithms, we can expand equations (6) in Taylor series to first order

$$\begin{aligned} TIHFC_{ij}(u_{kl}^{(m+1)}, v_{kl}^{(m+1)}, s_{kl}^{(m+1)}) &\approx TIHFC_{ij}(u_{kl}^{(m)}, v_{kl}^{(m)}, s_{kl}^{(m)}) + \\ &+ \frac{\partial TIHFC_{ij}(u_{kl}^{(m)}, v_{kl}^{(m)}, s_{kl}^{(m)})}{\partial u_{kl}^{(m)}}(u_{kl}^{(m+1)} - u_{kl}^{(m)}) + \\ &+ \frac{\partial TIHFC_{ij}(u_{kl}^{(m)}, v_{kl}^{(m)}, s_{kl}^{(m)})}{\partial v_{kl}^{(m)}}(v_{kl}^{(m+1)} - v_{kl}^{(m)}) + \\ &+ \frac{\partial TIHFC_{ij}(u_{kl}^{(m)}, v_{kl}^{(m)}, s_{kl}^{(m)})}{\partial s_{kl}^{(m)}}(s_{kl}^{(m+1)} - s_{kl}^{(m)}) \end{aligned}$$

where m is the iteration index. Employing the above equation and combining (6) and (8), we find a compact form of iterative equations as follows

$$\begin{pmatrix} u_{kl}^{(m+1)} \\ v_{kl}^{(m+1)} \\ s_{kl}^{(m+1)} \end{pmatrix} = \begin{pmatrix} u_{kl}^{(m)} \\ v_{kl}^{(m)} \\ s_{kl}^{(m)} \end{pmatrix} - \left(\mathbf{A}_{kl}^{(m)}\right)^{-1}\mathbf{B}_{kl}^{(m)} , (9)$$

where matrix $\mathbf{A}_{kl}^{(m)}$ and vector $\mathbf{B}_{kl}^{(m)}$ are defined by

$$\mathbf{A}_{kl}^{(m)} = \begin{pmatrix} (1+\lambda)\sum_{i,j\in\Omega}\left(\dfrac{\partial TIHFC_{ij}^{(m)}}{\partial u_{kl}^{(m)}}\right)^2 & \sum_{i,j\in\Omega}\dfrac{\partial TIHFC_{ij}^{(m)}}{\partial u_{kl}^{(m)}}\dfrac{\partial TIHFC_{ij}^{(m)}}{\partial v_{kl}^{(m)}} & \sum_{i,j\in\Omega}\dfrac{\partial TIHFC_{ij}^{(m)}}{\partial u_{kl}^{(m)}}\dfrac{\partial TIHFC_{ij}^{(m)}}{\partial s_{kl}^{(m)}} \\[3mm] \sum_{i,j\in\Omega}\dfrac{\partial TIHFC_{ij}^{(m)}}{\partial u_{kl}^{(m)}}\dfrac{\partial TIHFC_{ij}^{(m)}}{\partial v_{kl}^{(m)}} & (1+\lambda)\sum_{i,j\in\Omega}\left(\dfrac{\partial TIHFC_{ij}^{(m)}}{\partial v_{kl}^{(m)}}\right)^2 & \sum_{i,j\in\Omega}\dfrac{\partial TIHFC_{ij}^{(m)}}{\partial v_{kl}^{(m)}}\dfrac{\partial TIHFC_{ij}^{(m)}}{\partial s_{kl}^{(m)}} \\[3mm] \sum_{i,j\in\Omega}\dfrac{\partial TIHFC_{ij}^{(m)}}{\partial u_{kl}^{(m)}}\dfrac{\partial TIHFC_{ij}^{(m)}}{\partial s_{kl}^{(m)}} & \sum_{i,j\in\Omega}\dfrac{\partial TIHFC_{ij}^{(m)}}{\partial v_{kl}^{(m)}}\dfrac{\partial TIHFC_{ij}^{(m)}}{\partial s_{kl}^{(m)}} & (1+\lambda)\sum_{i,j\in\Omega}\left(\dfrac{\partial TIHFC_{ij}^{(m)}}{\partial s_{kl}^{(m)}}\right)^2 \end{pmatrix}$$

,

$$\mathbf{B}_{kl}^{(m)} = \begin{pmatrix} \sum_{i,j\in\Omega} TIHFC_{ij}^{(m)}\dfrac{\partial TIHFC_{ij}^{(m)}}{\partial u_{kl}^{(m)}} \\[3mm] \sum_{i,j\in\Omega} TIHFC_{ij}^{(m)}\dfrac{\partial TIHFC_{ij}^{(m)}}{\partial v_{kl}^{(m)}} \\[3mm] \sum_{i,j\in\Omega} TIHFC_{ij}^{(m)}\dfrac{\partial TIHFC_{ij}^{(m)}}{\partial s_{kl}^{(m)}} \end{pmatrix} ,$$

and

$$TIHFC_{ij}^{(m)} = T(i + u_{ij}^{(m)}\Delta t, j + v_{ij}^{(m)}\Delta t, t_2) - T_{ij}(t_1) + s_{ij}^{(m)} ,$$

where $\lambda \geq 0$ is a Levenberg-Marguardt factor that is adjusted at each iteration to guarantee that the matrix $\mathbf{A}$ is positive definite. A smaller value of the factor λ can be used, bringing the algorithm closer to the Gauss-Newton method with second order converging. This Levenberg-Marguardt method can improve converge properties greatly in practice and has become the standard of nonlinear least-squares routines.

The iteration equation (9) derived based on a more general form of TIHFC equation (2) contains a grouped terms. For most cases, if the grouped term in (2) is negligible (for well calibrated data), then a simplified form of the iterative equation with the DFD equation is given by

(a) Modeled Velocity Field   (b) Estimated Velocity Field
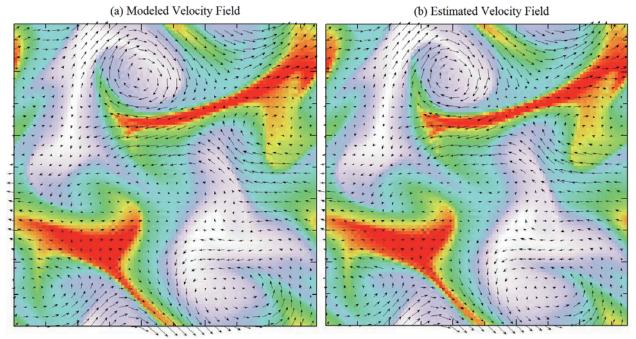

Figure 2. Velocity fields: (a) and (b) Average of the actual vector fields generated by the model at time $t_1 = 18$ hr and $t_2 = 20$ hr. (b) Estimated vector fields obtained by the new nonlinear inverse model from an image sequence between t_1 and t_2.

$$\mathbf{v}_{kl}^{(m+1)} = \mathbf{v}_{kl}^{(m)} - (\mathbf{a}_{kl}^{(m)})^{-1}\mathbf{b}_{kl}^{(m)}, \ (10)$$

where

$$\mathbf{a}_{kl}^{(m)} = \begin{pmatrix} (1+\lambda)\sum_{i,j\in\Omega}\left(\dfrac{\partial DFD_{ij}^{(m)}}{\partial u_{kl}^{(m)}}\right)^2 & \sum_{i,j\in\Omega}\dfrac{\partial DFD_{ij}^{(m)}}{\partial u_{kl}^{(m)}}\dfrac{\partial DFD_{ij}^{(m)}}{\partial v_{kl}^{(m)}} \\ \sum_{i,j\in\Omega}\dfrac{\partial DFD_{ij}^{(m)}}{\partial u_{kl}^{(m)}}\dfrac{\partial DFD_{ij}^{(m)}}{\partial v_{kl}^{(m)}} & (1+\lambda)\sum_{i,j\in\Omega}\left(\dfrac{\partial DFD_{ij}^{(m)}}{\partial v_{kl}^{(m)}}\right)^2 \end{pmatrix},$$

and

$$\mathbf{b}_{kl}^{(m)} = \begin{pmatrix} \sum_{i,j\in\Omega} DFD_{ij}^{(m)}\dfrac{\partial DFD_{ij}^{(m)}}{\partial u_{kl}^{(m)}} \\ \sum_{i,j\in\Omega} DFD_{ij}^{(m)}\dfrac{\partial DFD_{ij}^{(m)}}{\partial v_{kl}^{(m)}} \end{pmatrix}.$$

The local TIHFC equation (2) or DFD equation (3) is converted into a set of global simultaneous system equations in (8) by the bilinear expansion approach and the nonlinear least-squares principle, and they become local iterative equations in (9) or (10) again by the Gauss-Newton and Levenberg-Marguardt algorithms. All velocities on nodes can be solved by the iteration procedures based on the equation (9) or (10) that depends on image data type and calibrations.

The degree of the over-constraint parameter n can be adjusted to get from high to low resolutions of the structures for the velocity field. The effects of noise can be restrained efficiently by a higher degree of the over-determined equations in the nonlinear inverse model.

3. EXPERIMENTS

To assess the ability of the present method, we use the solution of a numerical model as a benchmark, and introduce a surface tracer field as an initial condition (see Chen *et al.*, 2008). Angular and magnitude measures of error are introduced in this section, and the mean values of these errors are applied to evaluate the performance of the velocity estimations.

3.1 Error Measurement

Angular and magnitude measures of error are used in this paper (Chen 2010). Velocity may be written as $\mathbf{v} = (u, v, 0)$ (assuming the component of velocity in z is $w = 0$), and then the angular and magnitude errors between the correct velocity $\mathbf{v}_c$ and an estimate $\mathbf{v}_e$ are

$$\Delta\theta = \arccos\left(\frac{\mathbf{v}_c \cdot \mathbf{v}_e}{|\mathbf{v}_c\|\mathbf{v}_e|}\right), \quad (11)$$

and

$$\Delta V = \frac{|\mathbf{v}_c - \mathbf{v}_e|^2}{|\mathbf{v}_c\|\mathbf{v}_e|}, \quad (12)$$

where magnitude errors are dimension-less quantity. The mean values of the angular and magnitude errors between the correct velocity $\mathbf{v}_c$ and an estimate $\mathbf{v}_e$ are used to evaluate the performance of the velocity estimations.

3.2 The Numerical Model

In order to demonstrate the performance of this new nonlinear inverse model for surface velocity estimation, a simulated flow field and its advection of sea surface temperature are obtained by solving 3D nonlinear fluid dynamical equations and the equation for the temperature. For the test, the temperature T is treated simply as a passive tracer with a weak diffusivity added for numerical stability (see Chen *et al.* 2008).

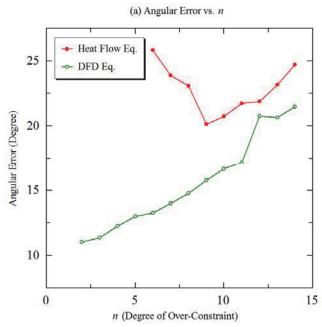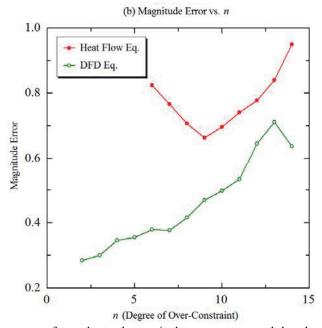(a) Angular Error vs. n

(b) Magnitude Error vs. n

Figure 3. Plots of error measurement generated by the linear and nonlinear inverse models with numerical model data at time $t_1 = 18$ hr and $t_2 = 20$ hr: (a) Mean values of angular error defined by the equation (11) vs. n (a degree of over-constraint), and (b) mean values of magnitude error defined by the equation (12) vs. n.

The inversion of the simulated SST for surface flow is performed using the nonlinear model for a range of node points. The number of pixels between two node points is defined by $n - 1$ as shown in Fig. 1. In terms of the number of node points, the smallest array size tested has the dimension of $2 \leq n \leq 14$ points on each side (see Fig. 3). In the calculations reported here for the numerical model data, only the heat flow without grouped terms in equation (10) is used.

The benchmark velocity vectors given by the numerical model are shown in Figure 2a. For comparison, vectors estimated by the nonlinear inverse model are shown in Figure 2b. The degree of over-constraint parameter n is assigned by two ($n = 2$). The false color presentation of images (96×96) in the background are the tracer fields (or simulated SST) with scales ranging from 0 to 50 (km) in horizontal and vertical, which by the time from 18 hr to 20 hr, has been deformed by the currents and is significantly different from its original $\sin(2\pi x / L)\sin(2\pi y / L)$ square cell shape.

The above comparisons between Fig. 2 (a) and (b) have been qualitative. Quantitative measures of how well the nonlinear inverse model can reproduce the simulation flow are seen in Fig. 3 in which the mean values of angular and magnitude error versus n ($n = n_x = n_y$) are shown. The two curves shown in Fig. 3 (a) and (b) demonstrate performance of both the linear inverse model (see Chen *et al*. 2008) and current nonlinear inverse model with the same velocity modelling and the global optimal strategies.

Both curves of angular and magnitude errors generated by the linear inverse model (see Chen *et al*. 2008) as shown in Fig. 3a and b (curves in red) exhibit a local minimum in the vicinity of $n \approx 9$, and two competing phenomena, one at small n and another for large n, are responsible for this. However, both

curves of angular and magnitude errors generated by the nonlinear inverse model shown in Fig. 3a and b (curves in green) decrease versus n until $n = 2$ continually. Values of both the angular and magnitude errors approach minimal points when the degree of over-constraint parameter n is equal to two as shown in Fig. 3. Both curves of angular and magnitude errors by the two methods clearly indicate that the current proposed estimator has much better performance than the linear inverse model (Chen *et al*. 2008) for the full range of n variation and particularly for the higher resolution of the velocity structure (small n).

3.3 Application to AVHRR Images

The intended application of the nonlinear inverse model with iterative equation in (10) is to obtain accurate estimation of the ocean surface velocity from AVHRR image sequences. We derived a velocity field from two NOAA satellite images taken in the New York Bight, east of the New Jersey coast and south of Long Island, NY. These data were taken on May 21, 2007 at times $t_1 = 10:46$ and $t_2 = 15:18$ UT. The pixel resolutions for the images are 1.008 (km) in the north-south and east-west directions. The temporal separations between images are thus $\Delta t = 4.32$ h. Level 2 sea surface temperature data which have been processed to remove sun glint, atmospheric aberrations, and geometric anomalies is used for these experiments. We calculated velocities from the AVHRR image sequence as shown in Fig. 4.

4. CONCLUSION

In this paper, a nonlinear model has been created for estimating velocity field under conservative constraint of the heat flow. The heat flow equation for surface velocity estimation is replaced by the temporal integral form of the heat flow constraint in which the initial and final states of motion terms are associated with only two time-varying frames at time t_1 and t_2. Gauss-Newton iterative equations with Levenberg-Marguardt algorithms for motion estimation are derived based on the temporal integral form of the heat flow equations, modelling the velocity field, and a nonlinear least-squares model.

The solution of a numerical model is used as a benchmark to exam the new estimator. Both angular and magnitude measures of error are applied to evaluate the performance of the velocity estimations from this numerical model image sequence. The new approach with the temporal integral form of the heat flow equations exhibits much better performance than the results by the same approach and numerical model using the heat flow equation. The algorithm performs very well even in the presence of the recording noise present in the realistic image sequences.

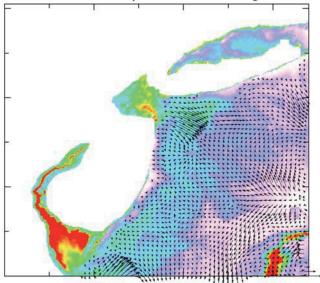Estimated Velocity Field from AVHRR Images

Figure 4. Vector field derived from the AVHRR image sequence (false color representation) from 10:46 to 15:18 UT on May 25, 2007 within unmasked region.

ACKNOWLEDGEMENTS

REFERENCES

Leese, J.A. and C.S. Novak, 1971, "An automated technique for obtaining cloud motion from geosynchronous satellite data using cross correlation," *J. Appl. Meteor.* vol. 10, no. 1, pp. 118-132.

Emery, W.J., A.C. Thomas, M.J. Collins, W.R. Crawford, and D.L. Mackas, 1986, "An Objective Method for Computing Advective Surface Velocities from Sequential Infrared Satellite Images," *J. Geophys. Res.*, vol. 91, pp. 12865-12878.

Horn, B. and B. Shunck, (1981), Determining optical flow, *Artificial Intelligence*, no. 17, 185–203.

Kelly, K. A., 1989, An Inverse Model for Near-Surface Velocity from Infrared Images, *J. Phys. Ocean.*, *19*,1845-1864.

Kelly, K. A., and P.T. Strub, (1992), Comparison of Velocity Estimates from Advanced Very High-Resolution, *J. Geophys. Res.*, vol. 97, 9653-9668.

Ostrovskii, A. G., and L. Piterbarg, (1995), Inversion for Heat Anomaly Transport from Sea-Surface Temperature Time-Series in the Northwest Pacific, *J. Geophys. Res.*, *100*, 4845-4865.

Ostrovskii, A. G., L.I. Piterbarg, (2000), Inversion of Upper Ocean Time Series for Entrainment, Advection, and Diffusivity, *J. Phys. Ocean.*, *30*, 201-204.

Vigan, X., C. Provost, R. Bleck R, and P. Courtier, (2000), Sea surface velocities from sea surface temperature image sequences 1. Method and validation using primitive equation model output, *J. Geophys. Res.*, *105*, 19499-19514.

Vigan, X., C. Provost, R. Bleck R, and P. Courtier, (2000), Sea Surface Velocities from Sea Surface Temperature Image Sequences 2.Application to the Brazil-Malvinas Confluence Area, *J. Geophys. Res.*, *105*, 19515-19534.

Zavialov, P.O., R.D. Ghisolfi, C.A.E. Garcia, (1998), An Inverse Model for Seasonal Circulation over the Southern Brazilian Shelf: Near-Surface Velocity from the Heat Budget," *J. Phys. Ocean., 28*, 545-562.

Cote, S. and A. R. L. Tatnall, (2007), The Use of the Hopfield Neural Network to Measure Sea-Surface Velocities From Satellite Images, *IEEE Geophys. Rem. Sens. Lett.*, 4, 4, pp. 624-628.

Marcello, J., F. Eugenio, F. Marqués, A. Hernández-Guerra, and A. Gasull, (2008), Motion Estimation Techniques to Automatically Track Oceanographic Thermal Structures in Multisensor Image Sequences, *IEEE Trans. Geosci. Rem. Sens.*, *Vol.* 46, *No* 9.

Lucas, B. D. and T. Kanade, (1981), An iterative image registration technique with an application to stereo vision, In DARPA Proc, of Image Understanding Workshop, pages 121-130.

Lucas, B. D., (1984), Generalized image matching by the method of differences, PhD thesis, Carnegie Mellon Univ.

Black, M.J. and Anandan, P., (1996), The robust estimation of multiple motions: parametric and piecewise smooth flow fields. *Computer Vision and Image Understanding*, 63(1):75–104.

Chen, W., R. P. Mied, and C. Y. Shen, (2008), Near-surface ocean velocity from infrared images: Global Optimal Solution to an inverse model, *J. Geophys. Res.*, 113, C10003, doi:10.1029/2008JC004747.

Chen, W., (2009), A Global Optimal Solution with Higher Order Continuity for the Estimation of Surface Velocity from Infrared Images, *Accepted to publish on IEEE Trans. Geosci. Rem. Sens*.

Chen, W., (2010), A Novel Criterion for Motion Detection and Segmentation, *Submitted for publication on IEEE Trans. TCSVT*.

Robbins, J. D. and A. N. Netravali, (1983), Recursive motion compensation: A review, in Image Sequence processing and Dynamic Scene Analysis, T. S. Huang, ed., pp. 76-103, Berlin, Germany, Springer-Verlag.